npj | Quantum Materials

www.nature.com/npjquantmats

ARTICLE OPEN

Check for updates

Multiorbital singlet pairing and $d+d$ superconductivity

Emilian M. Nica[1]✉ and Qimiao Si[2,3]✉

Recent experiments in multiband Fe-based and heavy-fermion superconductors have challenged the long-held dichotomy between simple *s*- and *d*-wave spin-singlet pairing states. Here, we advance several time-reversal-invariant irreducible pairings that go beyond the standard singlet functions through a matrix structure in the band/orbital space, and elucidate their naturalness in multiband systems. We consider the $s\tau_3$ multiorbital superconducting state for Fe-chalcogenide superconductors. This state, corresponding to a $d+d$ intra- and inter-band pairing, is shown to contrast with the more familiar $d+id$ state in a way analogous to how the B- triplet pairing phase of ^{3}He superfluid differs from its A- phase counterpart. In addition, we construct an analog of the $s\tau_3$ pairing for the heavy-fermion superconductor $CeCu_2Si_2$, using degrees-of-freedom that incorporate spin-orbit coupling. Our results lead to the proposition that *d*-wave superconductors in correlated multiband systems will generically have a fully-gapped Fermi surface when they are examined at sufficiently low energies.

npj Quantum Materials (2021)6:3 ; https://doi.org/10.1038/s41535-020-00304-3

INTRODUCTION

Unconventional superconductivity of strongly correlated systems is centrally important in condensed matter physics, with the symmetry of the superconducting order parameter being a key issue of the field. This question appears to have reached a consensus in some notable instances. An example is the *d*-wave symmetry for the Cooper pairs in the well-studied Cu-based superconductors (SCs)[1,2]. However, the pairing symmetry remains enigmatic in other classes of strongly correlated materials. For singlet superconductivity, the long-held dichotomy is between fully-gapped *s*- and nodal *d*-wave pairing states. However, it has been increasingly recognized that multi-band/orbital systems are inherently richer for pairings[3,4]. A canonical setting for multiorbital spin-singlet pairings is the Fe-based superconductors[5–11], especially for the Fe-chalcogenide cases. Here, the discovery of an orbital-selective Mott crossover in the normal state[12,13] motivated the notion of orbital-selective superconductivity[14]. The latter opens up the possibilities for a variety of orbital-dependent pairing states, which have been studied in recent years both theoretically[15–20] and experimentally[21–23]. In addition, heavy fermion SCs, a class that includes about fifty members, have emerged as another prominent setting for singlet pairing states beyond the traditional possiblities[24].

Recent experiments have directly challenged the conventional *s*- and *d*-wave dichotomy. In alkaline Fe-selenides, inelastic neutron scattering[25,26] revealed signatures of in-gap spin resonances, whose characteristic wavevectors qualify them as a typical indicator of sign-changing *d*-wave order parameters[7,9,27–29]. By contrast, ARPES studies have indicated fully-gapped superconductivity[30–33], even for a Fermi pocket near the center of the two-dimensional Brillouin zone (BZ), which appears consistent with *s*- wave symmetry. Understanding the Fe-chalcogenide SC is crucially important, since the Fe-based superconductivity with the highest superconducting transition temperature (T_c) occurs in this category.

A similar situation has emerged in the heavy-fermion system $CeCu_2Si_2$ (Ref. [34]). A host of properties, including the inelastic neutron-scattering spectrum[28], have traditionally been interpreted in terms of a sign-changing *d*-wave pairing state, yet recent specific heat[35] and London penetration depth[34,36] results at very low temperatures pointed toward a fully gapped Fermi-surface (FS).

It is surprising that the SC phases exhibit *s*- and *d*-wave characters simultaneously. One possible origin is $s+id$ pairing, which breaks the point-group (PG) and time-reversal (TR) symmetries. While TR symmetry breaking may develop in special instances in the bulk[37] or on the surface[38], FeSCs typically preserve TRS. Especially for the alkaline Fe-selenides, there is no evidence for either TR symmetry-breaking or two-stage phase transitions as the temperature is lowered. Thus, it is important to identify an alternate candidate pairing. For the Fe-chalcogenide SC, one candidate pairing state was named $s\tau_3$[17]. It has the $s-$waveform factor, but τ_3, a Pauli matrix in the *xz*, *yz* 3*d*-electron orbital basis, turns the pairing state into $d-$wave-like; indeed, in the band basis, the $s\tau_3$ pairing has the intra- and inter-band $d+d$ form. That both intra- and inter-band pairings can play a role is to be expected in this type of model[39] and other cases[4,40]. However, this $d+d$ form is highly unusual, thereby raising the question of both its naturalness and generality.

With the stage set by the above, the present work makes two advances. First, we demonstrate that the $d+d$ pairing state belongs to matrix singlet pairing order parameters with non-trivial orbital structures that are natural and likely common-place in multi- orbital/band systems. As the orbital degrees-of-freedom (DOF) transform non-trivially under PG operations, these matrices can be chosen as one of the irreducible representations of the same group.

We make a case for the matrix singlet pairing's naturalness by presenting an in-depth analysis of the $s\tau_3$ pairing state. Written in the band basis, the $s\tau_3$ pairing has the intra- and inter-band $d+d$ form, but it remains an irreducible B_{1g} representation of the (tetragonal D_{4h}) PG. The unusual $d+d$ pairing state is to be contrasted with its more commonly discussed $d+id$ counterpart. Nonetheless, it is well defined. We demonstrate this point by showing that the $d+d$ singlet pairing state can be compared and contrasted with the more familiar $d+id$ state in analogy with how, in the case of superfluid ^{3}He, the well-defined B-phase is measured against the equally well-known A-phase. The latter are

[1]Department of Physics, Arizona State University, Box 871504, Tempe 85287-1504 AZ, USA. [2]Department of Physics and Astronomy, Rice University, 6100 Main St, Houston 77005 TX, USA. [3]Rice Center for Quantum Materials, Rice University, 6100 Main St, Houston 77005 TX, USA. ✉email: enica@asu.edu; qmsi@rice.edu

spin-triplet pairing states that have an inherent matrix structure—in spin space—even for single-band cases.

Second, we illustrate the matrix singlet pairing's generality by constructing this type of state in other multiband systems, for the case of heavy fermion superconductor $CeCu_2Si_2$. This is an important undertaking, given that $CeCu_2Si_2$ is the first-ever discovered unconventional SC[41], and also recognizing that heavy fermion systems represent a prototype setting for strong correlations and unconventional superconductivity in general[42–44]. Using DOF that incorporate spin-orbit coupling (SOC), we introduce an $s\Gamma_3$ state. This provides the theoretical basis for the excellent description of the experimental results in $CeCu_2Si_2$ in terms of the $d+d$ pairing order parameter[24,34].

We will for the most part direct our analysis towards the effect of multiple orbitals/bands on the nature of the pairing states. Therefore, the issue of what drives such pairing states in the multi-orbital/band settings will only be briefly considered. Where this is done, our emphasis is on the short-range spin exchange interactions that are themselves induced by the underlying Coulomb (Hubbard and Hund's) interactions. What we have achieved, from these microscopic calculations, is to demonstrate the relevance of the general considerations given above. We expect that our calculation will motivate further microscopic studies that include additional microscopic physics, such as orbital fluctuations, or are based on other approaches to the electron-correlation effects.

The emphasis of the present work is on singlet pairing states. Triplet pairing already has a matrix form that transforms nontrivially in spin space, even for single-band systems such as ^{3}He. However, candidate solid state systems for triplet pairing often involve multiple orbitals/bands and strong correlations[45–50]. Thus, the type of matrix pairing structure in the orbital/band space we consider here may produce triplet superconducting states[51,52] and the associated excitations that are of potential interest to quantum computing.

The remainder of the paper is organized as follows. We begin the first subsection of our results by discussing some of the most relevant general properties of non-trivial matrix pairing in the context of the Fe-based SCs. We subsequently define the $s\tau_3$ pairing, and discuss the unusual properties of this state and show how it can be stabilized in an s- to d-wave degeneracy regime. We also support our discussion with numerical results for the pertinent five-orbital models of the Fe-based SCs. Furthermore, we consider $s\tau_3$ in the band basis and illustrate how it is analogous to ^{3}He -B. In the second subsection, we contrast the multiband $d+d$ intra- and inter-band pairing state with the single-band $d+id$ pairing state, and argue that these two cases are the analogs of ^{3}He B and A. We show how they can be stabilized in a $t-J_1-J_2$ model. In the third subsection, we extend the notion of non-trivial orbital structure beyond the Fe-based compounds by discussing a candidate analogous to $s\tau_3$ for the heavy-fermion SC $CeCu_2Si_2$. In order to clearly see these results, we also present the irreducible representations of the D_{4h} point group in the context of $CeCu_2Si_2$. The Methods section contains additional accounts of the numerical results which support the stability of $s\tau_3$ pairing for the alkaline Fe-selenides. We also discuss the $t-J$ model and its solutions which illustrate the case of $d+id$ pairing. Additional important aspects of matrix pairing are discussed in the Supplementary Notes. There, for completeness, we outline the role of the matrix-pairing functions in the various phases of superfluid ^{3}He, where spin provides the analog of the orbital DOF. We highlight the lessons we believe can be applied to the case of multiorbital pairing in unconventional SCs. In addition, we illustrate how s- and d-wave states can coexist without breaking either PG or TR-symmetries via a general Landau-Ginzburg analysis. The band-basis representation of $s\tau_3$ pairing and an illustration of the effects of damping on Bogoliubov-de Gennes (BdG) quasiparticles are also presented in the Supplementary Notes.

RESULTS

$d+d$ matrix singlet pairing as an analog of ^{3}He -B

In solid-state systems, electrons inherit the orbital structure of the underlying ions which form the crystalline lattice. The set of local DOF must include the additional orbital structure. In turn, Cooper pairs formed out of the same electrons are naturally characterized by these additional local, orbital DOF.

Consider the concrete case of an electronic system on a lattice with D_{4h} tetragonal point-group symmetry. Further, assume that the dominant contribution to the lowest-lying bands is due to xz and yz orbital local DOF. For simplicity, we ignore SOC. In general, the pairing interactions $V(\mathbf{k},\mathbf{k}')_{\alpha\beta;\Gamma\delta}$ depend on the momenta as well as the orbital and spin indices of the two electrons. This two-dimensional space turns out to be relevant for Fe-based SCs [53–55], and we will first define the $s\tau_3$ pairing state in this space. The pairing is orbitally selective in that it is intraorbital and its amplitude is orbital dependent. We will then consider the stability of the matrix singlet pairing state in more realistic five-orbital models. Through the $d+d$ representation in the band basis, we present an intriguing analogy of the singlet pairing state as an analog of ^{3}He -B.

Matrix pairing in multiorbital Fe-based SCs. A spin-singlet pairing restricted in the orbital space to the xz, yz cubic harmonics will have the general form

$$\hat{\Delta}(\mathbf{k}) = \Delta \hat{g}(\mathbf{k})_{\alpha\beta} i\sigma_2. \tag{1}$$

The even-parity matrix $\hat{g}(\mathbf{k})$ denotes the components of the pairing in the four-dimensional space spanned by the tensor products of the two orbital DOF. These tensor-product states are analogs to the spin-1/2 product states in triplet ^{3}He (see Supplementary Note 1). Likewise, they depend on the relative momentum of the pair. Finally, $i\sigma_2$ denotes spin-singlet pairing. We do not consider this additional structure since it plays no essential role in the subsequent discussion.

The pairing matrix can be decomposed into components which transform according to one of the five even-parity irreducible representations of the D_{4h} point group. This allows for additional separation of the DOF as

$$\hat{g}^{(i)}(\mathbf{k})_{\alpha\beta} = g^{(i)}(\mathbf{k})\hat{\tau}^{(i)}_{\alpha\beta}, \tag{2}$$

where i labels one of the five, even-parity $A_{1g}, A_{2g}, B_{1g}, B_{2g}$, and E_g irreducible representations of D_{4h}. The functions $g^{(i)}(\mathbf{k})$ can likewise be chosen to belong to one of these representations. To illustrate, s-wave states such as $s_{x^2+y^2}(\mathbf{k})$ and $s_{x^2y^2}(\mathbf{k})$ both belong to A_{1g}. Standard d-wave states such as $d_{x^2-y^2}(\mathbf{k})$ and $d_{xy}(\mathbf{k})$ are B_{1g} and B_{2g} representations, respectively. The xz, yz orbital doublet transforms as the two-component E_g representation. The $\tau^{(i)}_{\alpha\beta}$ identity and Pauli matrices describe linear combinations of the tensor-product states which transform according to one of four irreducible representations contained in the $E_g \times E_g = A_{1g} + A_{2g} + B_{1g} + B_{2g}$ decomposition of the tensor-product space of the two E_g orbital DOF. By analogy to the total $S=1$ spin states of ^{3}He, these matrix-elements play the role of effective Clebsch-Gordan coefficients. The τ_0, τ_1, and τ_3 matrices transform according to A_{1g}, B_{2g}, and B_{1g}, respectively. In this work, we consider parity-even spin-singlet pairings belonging to one-dimensional irreducible representations of D_{4h}. This naturally excludes pairing states involving τ_2 matrices, which would be parity-odd.

These arguments point to an important aspect. In ^{3}He, the relative angular momentum and local (spin) DOF transform independently under separate groups. In the present case, $g^{(i)}(\mathbf{k})$ and orbital matrix parts ($\tau^{(i)}$) are necessarily coupled since they both transform under the same PG. In effect, this constitutes an inherent SOC-like locking of the different spatial DOF of the Cooper pair.

We note that the single-component representation pairings in Eqs. (1) and (2) are unitary such that

$$\hat{\Delta}^{\dagger}(\mathbf{k})\hat{\Delta}(\mathbf{k}) = \Delta^2 g^2(\mathbf{k})\tau_0. \tag{3}$$

Of particular relevance to our discussion is the fact that pairing with non-trivial matrix structure in general allows for several inequivalent representations of the PG. The problem of determining the stability of the different pairings, including those with non-trivial structure, is a challenging task, which is typically treated numerically on a case-by-case basis. We illustrate this point further below in this section, within a five-orbital t-J_1-J_2 model.

$s\tau_3$ pairing state. Of interest here is the $s\tau_3$ pairing. In terms of Eqs. (1) and (2), it corresponds to

$$g(\mathbf{k}) = s_{x^2y^2}(\mathbf{k}) \tag{4}$$

$$\hat{\tau}_{\alpha\beta} = \tau_{3,\alpha\beta}. \tag{5}$$

It transforms as the B_{1g} representation due exclusively to the τ_3 matrix. Because of the orbital struture, it represents neither simple s- nor d-wave states. However, $s\tau_3$ pairing preserves both PG- and TR-symmetries of the normal state.

To illustrate the properties of the $s\tau_3$ pairing, we first consider a simplified two-orbital model[53] and neglect any possible subleading channels. The TB and pairing parts of the BdG Hamiltonian in the orbital basis read[39]

$$\hat{H}_{\mathrm{BdG}}(\mathbf{k}) = \hat{H}_{\mathrm{TB}}(\mathbf{k}) + \hat{H}_{\mathrm{Pair}}(\mathbf{k}) \tag{6}$$

$$\hat{H}_{\mathrm{TB}}(\mathbf{k}) = [(\xi_0(\mathbf{k}) - \mu)\tau_0 + \xi_1(\mathbf{k})\tau_1 + \xi_3(\mathbf{k})\tau_3] \otimes \gamma_3 \tag{7}$$

$$\hat{H}_{\mathrm{Pair}}(\mathbf{k}) = \Delta(k)s_{x^2y^2}(\hat{\mathbf{k}})\tau_3 \otimes \gamma_1. \tag{8}$$

The γ Pauli matrices act in Nambu space. To simplify the expressions, we discuss one of the two spin-sectors. With singlet pairing, the Hamiltonian for the other sector can be obtained in straightforward fashion. Note that, from the perspective of point-group symmetry classification, $s\tau_3$ transforms in the same B_{1g} representation as the diagonal-in-orbital-space $d_{x^2-y^2}\tau_0$ pairing, as has been discussed in this type of model[39] and related settings[56–59]. What distinguishes the $s\tau_3$ pairing is the nontrivial commutation relation between the corresponding pairing and kinetic parts of the Hamiltonian[17].

It is instructive to recognize that the $\xi_1\tau_1$ and $\xi_3\tau_3$ terms of $\hat{H}_{\mathrm{TB}}$ play a role similar to a Rashba SOC. The bands corresponding to the normal-state dispersion are

$$\epsilon_{\pm}(\mathbf{k}) = \xi_0(\mathbf{k}) \pm \sqrt{\xi_1^2(\mathbf{k}) + \xi_3^2(\mathbf{k})}, \tag{9}$$

reflecting the space-group allowed varying orbital-content and splitting of the Fermi surfaces (FSs). We refer the reader to "Pairing channels of the five-orbital $t-J_1-J_2$ model" subsection in Methods for detailed expressions of the ξ's. The FS corresponding to this effective model has electron pockets centered at the $(\pm\pi, 0)$ and $(0, \pm\pi)$ points of an one-Fe unit cell.

In Ref. [17], we showed that the general BdG dispersion is *always gapped along the FS*. Nodes away from the FS can appear for larger band splitting[17,60,61], reflecting the corrections to the gap term due to the non-commuting TB and pairing parts. However, in alkaline-Fe selenides, where $s\tau_3$ pairing is competitive, the small band splitting at the center of the Brillouin zone precludes the appearance of nodes. Even in the cases when the nodes were to appear in the BdG spectrum away from the Fermi surface, it will not affect our conclusion. The point is that, in strongly correlated systems, only nodal excitations on the Fermi energy are long lived and, thus, sharply defined. For states away from the Fermi energy, any putative nodal excitations will necessarily involve a large damping caused by the underlying electron correlations, which obviates the distinction between nodal and gapped excitations. We illustrate how this can occur in Supplementary Note 5.

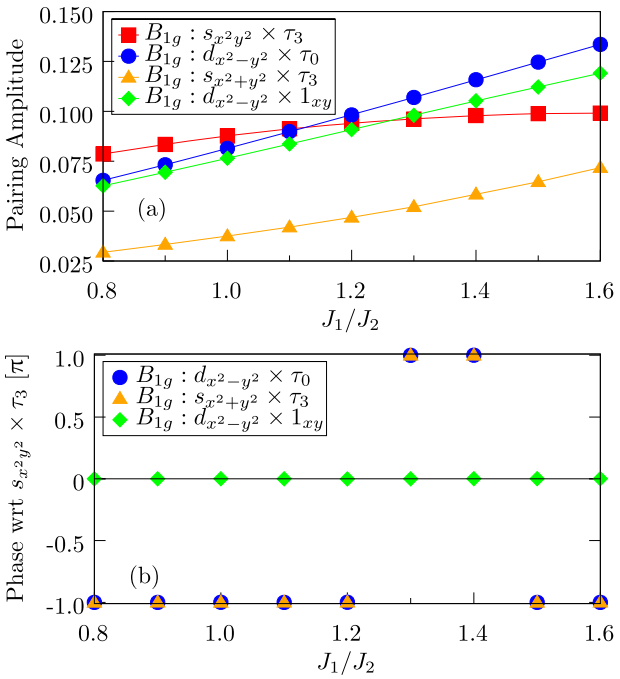

Fig. 1 Zero-temperature results for a five-orbital $t-J_1-J_2$ model. **a** Dimensionless pairing amplitudes of the leading B_{1g} channels as compared to that of the B_{1g} $s\tau_3$ channel as functions of J_1/J_2 for a five-orbital $t-J_1-J_2$ model of the alkaline Fe-selenides. The numerically-determined pairing amplitudes are the weights of each of the PG symmetry-allowed channels. $\mathbf{1}_{xy}$ denotes the trivial 1×1 matrix in the d_{xy} orbital sector. See subsections "Pairing channels of the five-orbital $t-J_1-J_2$ model" and "Five-orbital $t-J_1-J_2$ model and solution method" in Methods for the details of the calculation. The $s\tau_3$ pairing with non-trivial orbital structure is dominant in the $0.8 \le J_1/J_2 \le 1.0$ window. **b** Phases of the leading B_{1g} channels relative to the $s\tau_3$ channel as functions of the tuning parameter. These are obtained from the difference in the phases of each symmetry-allowed channel which are determined from the self-consistent solution. In the [0.8, 1] interval where $s\tau_3$ is dominant, these relative phases are either zero or $\pm\pi$. Here, the amplitudes of the coexisting B_{1g} channels are comparable to that of $s\tau_3$. This illustrates that the $s\tau_3$ pairing which is equivalent to $d+d$, effectively preserves TR and PG symmetries.

Another important characteristic of such a gapped $s\tau_3$ state is its sign change under a $\pi/2$ rotation. Such a sign-change leads to the formation of an in-gap spin resonance. $s\tau_3$ is then a pairing state which reconciles a fully-gapped FS with the presence of a spin-resonance, typically associated with a $d-$wave gapless order parameter.

Although we focus on a simplified two-orbital model in order to illustrate the salient properties of $s\tau_3$ pairing, the latter can also be stabilized in more general five-orbital models of the alkaline Fe-selenide class of SCs. The pairing matrix in the $t-J_1-J_2$ model can be decomposed into all the symmetry-allowed channels. The complex coefficients of these components have both amplitude and phase. The illustrative results are shown in Fig. 1a, b. The zero-temperature pairing amplitudes of all symmetry-allowed pairing channels have been determined in a five-orbital $t-J_1-J_2$ model with nearest and next-nearest exchange couplings. This model and its solution method are discussed in subsection "Five-orbital $t-J_1-J_2$ model and solution method" in Methods section.

The TB part and the associated FS are chosen to be consistent with LDA studies[17]. The dominant pairing amplitudes are intra-orbital.

The pairing state is orbital selective in the sense that the pairing amplitude and its phase are orbital sensitive. We focus on the case where the pairing amplitude is largest for the *xz*, *yz* orbitals while also allowing inter-orbital pairing. This reflects orbital-selective correlation effects in the normal state. The J_1/J_2 ratio controls the symmetry of the dominant pairing channel with $s_{x^2y^2}(\mathbf{k})\tau_0$ and $d_{x^2-y^2}(\mathbf{k})\tau_0$ states for small and large values of the ratio, respectively. The $s\tau_3$ pairing is dominant near the transition separating order-parameters belonging to A_{1g} to B_{1g} representations for a finite range of the control parameter about the point where $J_1/J_2 \approx 1$. A $d_{x^2-y^2}\tau_0$ with trivial orbital structure provides the subleading pairing with comparable amplitude. See subsection "Pairing channels of the five-orbital $t-J_1-J_2$ model" of the Methods for more details.

It is important to put the results of microscopic studies in a more general perspective. Our calculations indicate that a subleading $d_{x^2-y^2}\tau_0$ pairing of comparable amplitude is present in the regime where $s\tau_3$ is dominant. While we have focused on the properties of the dominant $s\tau_3$ pairing alone, a more realistic picture would involve coexisting $s\tau_3$ and $d_{x^2-y^2}\tau_0$ in the vicinity of *s*- to *d*-wave phase transition. This superposition of pairing states with different orbital structure which belong to the same B_{1g} irreducible representation preserves both PG- and TR-symmetries. In Supplementary Note 3, we present a Landau-Ginzburg analysis to show that, generically, the pairing state involves a linear superposition of these two components and there is only one superconducting transition at a single T_c.

Intra- and inter-band d + d *pairing and its analogy with the* ^{3}*He B-phase.* It is instructive to consider the $s\tau_3$ pairing in a band basis:

$$\hat{H}_{\text{Pair}}(\mathbf{k}) = \Delta_3(\mathbf{k})a_3 + \Delta_1(\mathbf{k})a_1, \tag{10}$$

where $a_{1,3}$ are Pauli matrices in the two-band space and where the form factors $\Delta_{3,1}$ transform as $d_{x^2-y^2}$ and d_{xy}, respectively. The details of the transformation from orbital to band basis are discussed in Supplementary Note 4. There, we also show that the $a_{3,1}$ matrices are equivalent to A_{1g} and A_{2g} representations, respectively, by applying the inverse transformation from band to orbital basis. The same conclusion can be reached by requiring that each of the two terms in Eq. (10) transforms as B_{1g}. Because the overall pairing is in the irreducible B_{1g} channel, it is natural that the intraband a_3 part has the $d_{x^2-y^2}$ form factor. Likewise, the interband a_1 component has the d_{xy} form factor. Thus, the $s\tau_3$ pairing is equivalent to a $d+d$ pairing.

When the pairing matrix is squared, the intra- and inter-band *d*-waves add in quadrature as $\Delta_1^2(\mathbf{k}) + \Delta_2^2(\mathbf{k})$ to produce a gap which does not close along the FSs centered on the BZ center corresponding to the two bands, as shown in Fig. 2. This is due to the anti-commuting nature of the two Pauli matrices a_3 and a_1 which denote intra- and inter-band pairing, respectively. As in the orbital basis, corrections to this gap are present due to the splitting of the FSs. As discussed in the previous subsection, in cases relevant to our discussion, these additional effects are typically small and consequently do not close the gap; and generically, the FS is always fully gapped.

The band basis reveals a pairing structure which is very similar to that in ^{3}He -B. Referring to Supplementary Notes 1 and 2, the matrix order-parameter in that case is typically expressed as $\hat{\Delta}_{^3\text{He}-\text{B}}(\mathbf{k}) \sim (\mathbf{k}\cdot\boldsymbol{\sigma})i\sigma_2$. This amounts to a linear superposition of *p*-wave states, p_x, p_y and p_z, together with a matrix structure made possible due to spin-triplet pairing as represented by the $\boldsymbol{\sigma}$ Pauli matrices. The anti-commuting nature of these matrices ensures that three *p*-waves add in quadrature to produce a full gap. The situation clearly mirrors the case of $s\tau_3$ in the band basis, where two *d*-wave states likewise produce a finite gap. The $s\tau_3$ pairing thus provides a remarkable example where a phase which is similar to ^{3}He -B via a structure in the band-basis is stabilized in a solid-state SC model.

Along with this similarity between the $s\tau_3$ pairing state and the B phase of ^{3}He, it is important to also note on the ways in which they differ. The distinctions are due primarily to the continuous rotation symmetries of ^{3}He as contrasted with the discrete nature of the PG in the inter- and intra-band *d*-wave case. The latter belong to a single irreducible representation of a PG involving discrete operations. As such, they break no symmetries of the normal state with the trivial exception of a global phase rotation due to pairing. By contrast, ^{3}He -B breaks the $SO(3)_{\mathbf{L}} \times SO(3)_{\mathbf{S}}$ symmetry of the normal state down to $SO(3)_{\mathbf{L}+\mathbf{S}}$, via a relative spin-orbit symmetry breaking[62,63]. Specifically, the invariance of the normal state under *continuous and independent* rotations of angular-momentum and spin, respectively, is broken down to simultaneous rotations in both sectors. In spite of this additional symmetry-breaking, we note that the B phase has the largest residual symmetry of all superfluid ^{3}He phases. In this respect, it still resembles intra- and inter-band *d*-wave pairing which preserves both PG and TR symmetries.

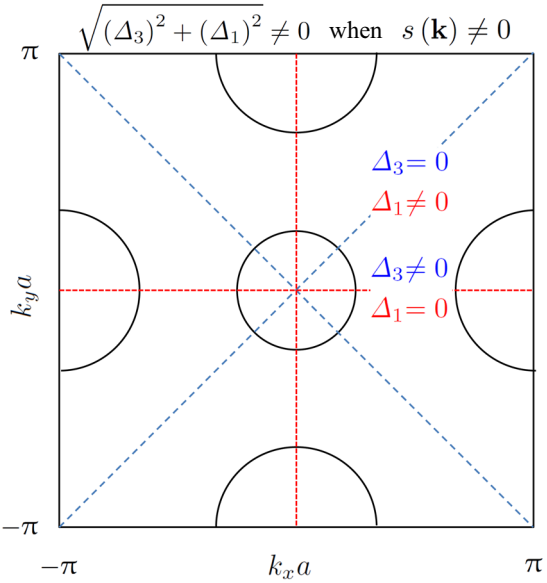

Fig. 2 The gapping of an illustrative FS by $d+d$ pairing. The blue, dashed line indicates the nodes of the intra-band component Δ_3 (Eq. (10)), which transforms as a B_{1g} representation of D_{4h}. The red, dotted line shows the nodes of the inter-band component Δ_1 (also in Eq. (10)), which transforms as a B_{2g} representation. The two components add in quadrature to produce a nonzero gap everywhere on the FS. Note that possible nodes of a common *s*-wave form factor (Eqs. 28-29 of Supplementary Note 4 for $s\tau_3$) are not shown here as they are irrelevant to our argument.

$d+d$ and $d+id$ pairing: Analogy with ^{3}He -B *vs.*^{3}He -A

We have seen that an orbital basis is convenient for classifying the pairing states according to symmetry and for solving microscopic models. Physically, the equivalent band basis is more natural in connecting with experiments. We have also seen that the non-trivial $s\tau_3$ pairing is equivalent to simultaneous intra- and inter-band $d_{x^2-y^2}$ and d_{xy} pairings (Eq. (10)). These add in quadrature to produce a full gap on the FS on either of the two bands and their sign-changing factors allow for the formation of in-gap spin resonances. For simplicity, we consider only unitary pairings. The intra- and inter-band terms are consequently associated with a_3 and a_1 Pauli matrices, respectively. Importantly, a $d+d$ pairing does not break either PG or TR symmetries of the Hamiltonian. This amounts to associating both *d*-wave components with a single irreducible representation in an orbital basis.

We have shown that the $d+d$ pairing is a well-defined pairing state, through an analogy with the B phase of ^{3}He. To further elucidate the naturalness of this unusual pairing state, we compare and contrast it with the more familiar $d+id$ pairing. We show that $d+d$ *vs.* $d+id$ pairing is analogous to the B- *vs.* A-phases of ^{3}He.

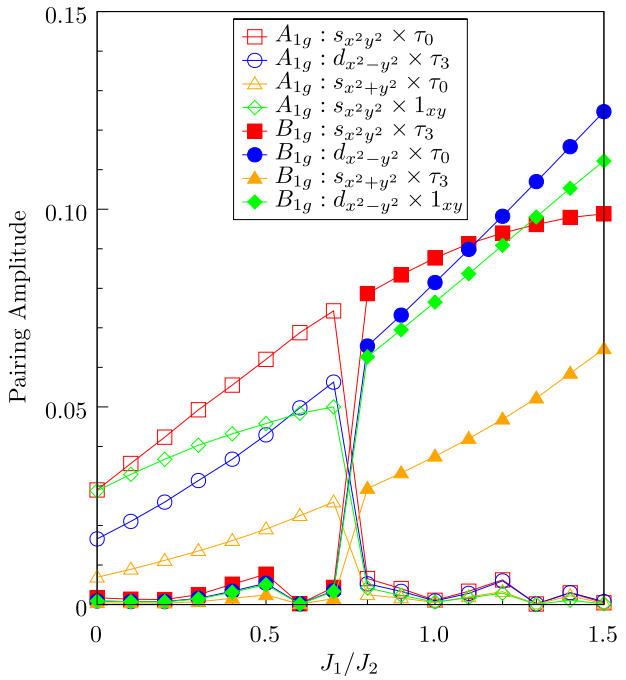

Fig. 3 Zero-temperature leading pairing amplitudes (dimensionless) as functions of $J_1^{xz/yz}/J_2^{xz/yz}$ for a five-orbital $t-J_1-J_2$ model of the alkaline Fe-selenides. $J_2^{xz}=J_2^{yz}=1/2$ in units of the bandwidth. The exchange interactions for the d_{xy} orbital are five times smaller while the exchange couplings for all remaining orbitals are zero. Please see Ref. [17] for a detailed account of the model and solution. For $J_1/J_2 \leq 0.7$ A_{1g} pairing channels are dominant with leading $s_{x^2y^2}\tau_0$ in the *xz*/*yz* sector. This pairing has trivial orbital structure. There is a narrow region of coexistence between finite A_{1g} and B_{1g} channels for $0.7 \leq J_1/J_2 \leq 0.8$. Beyond this range, B_{1g} channels dominate with leading $s_{x^2y^2}\tau_3$ in the *xz*/*yz* sector which has non-trivial orbital structure. At even larger values, an orbital-trivial $d_{x^2-y^2}\tau_0$ phase dominates.

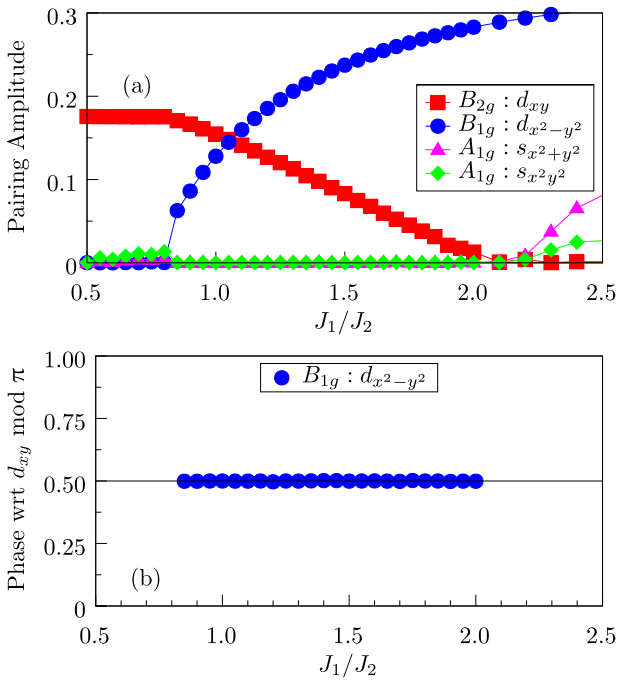

Fig. 4 Zero-temperature results for a single-orbital $t-J_1-J_2$ model close to half-filling. See subsection "Single-orbital $t-J_1-J_2$ model" of the Methods for details of the model. (a) Dimensionless pairing amplitudes as functions of the ratio J_1/J_2. When the tuning parameter is less than 0.8, only the d_{xy}, B_{2g} channel has finite amplitude. In the $0.8 \leq J_1/J_2 \leq 2.1$ interval, d_{xy} coexists with a $d_{x^2-y^2}$, B_{1g} channel. For larger values of the tuning parameter, the d_{xy} channel is suppressed and $s_{x^2+y^2}$ and $s_{x^2y^2}$ A_{1g} channels emerge. (b) Relative phase of the two *d*-wave channels modulo π as a function of J_1/J_2. When both *d*-waves have finite amplitudes, a $\pi/2$ relative phase is clearly visible. When one of the two is suppressed, the relative phase is essentially arbitrary.

d + d *in a multiorbital model* vs. d + i*d in a single-orbital model*. An *intra-band* $d+id$ pairing, where the two components are $d_{x^2-y^2}$- and d_{xy}-waves, respectively, is a natural competitor to the intra- and inter-band $d+d$. Here, we show how the intra-band $d+id$ can be stabilized in a one-band $t-J_1-J_2$ model in the vicinity of the $J_1 \approx J_2$ point.

In the first subsection, we discussed how the $s\tau_3$ orbital non-trivial pairing channel becomes dominant for a finite range of the J_1/J_2 tuning parameter in a realistic five-orbital $t-J_1-J_2$ model for the alkaline Fe-selenides. The details of the calculations are given in the Methods section. We showed how $s\tau_3$ pairing is equivalent to a $d+d$ intra- and inter-band pairing. To further understand the nature of the $s\tau_3$ -dominated state, we plot the phases of the leading B_{1g} channels relative to $s\tau_3$ as functions of J_1/J_2 in Fig. 1 (b). The leading B_{1g} channels have relative phases wrt $s\tau_3$ which are closely centered around 0 or π for the entire range of the tuning parameter. In the [0.8, 1] interval where $s\tau_3$ is dominant the relative phases are either zero or $\pm\pi$. Here the amplitudes of the subleading $d_{x^2-y^2}\tau_0$ and $s_{x^2+y^2}\tau_3 B_{1g}$ channels are comparable to that of the leading $s\tau_3$. Therefore, this regime corresponds to a pairing state with non-trivial orbital structure which preserves TR and PG symmetries. We note that all A_{1g} and B_{2g} channels are strongly suppressed in the regime where $s\tau_3$ is dominant which we consider here (Fig. 3).

We next discuss the orbital-trivial $d+id$ pairing. For simplicity, we consider a single d_{xy} orbital $t-J_1-J_2$ model on a square lattice. We choose the tight-binding (TB) parameters and chemical potential to be consistent with a circular hole pocket at the center of the BZ. The details of the model are discussed in subsection "Single-orbital $t-J_1-J_2$ model" of the Methods. The model is solved using a self-consistent decomposition of the exchange interactions as in the five-orbital cases discussed previously[17,64]. The resulting zero-temperature pairing amplitudes for $J_2=1/2$ in units of the bandwidth, and for a finite range of the ratio J_1/J_2 are shown in Fig. 4a. For $J_1/J_2<0.8$, the only significant pairing occurs in the d_{xy}, B_{2g} channel. For higher values of J_1/J_2, the amplitude of a $d_{x^2-y^2}$, B_{1g} pairing becomes finite. These two remain finite up to $J_2/J_1 \approx 2.1$, where the d_{xy} component vanishes continuously. Beyond this point, two additional $s_{x^2+y^2}$ and $s_{x^2y^2}$ order-parameters emerge. A similar conclusion has been reached in a related model[65].

To illustrate that the two coexisting *d*-wave components are locked into a $d+id$ state, we plot their relative phases mod π in Fig. 4b. The relative phases are obtained from the difference in the phases of each symmetry-allowed channel which are determined from the self-consistent solution. While these relative phases are essentially arbitrary whenever one of the *d*-waves vanishes, a $\pi/2$ relative phase is clear in the interval $J_1/J_2 \in [0.8, 2.1]$ where both coexist. Although these results were obtained for a single-orbital model, they do demonstrate how a $d+id$ pairing with trivial orbital structure can become stable in similar two-orbital models.

d + d *pairing* vs. d + i*d: Analogy with B- vs. A-phases of* ^{3}*He superfluid*. In the first subsection, we showed that the $d+d$ pairing is closely analogous to the B phase of ^{3}He, where the pairing is a superposition of $p_{x,y,z}$-waves corresponding to equal- and opposite-spin pairing as illustrated by Eqs. 2 and 3 of Supplementary Notes 1 and 2. Just like the B phase, the $d+d$ pairing is an irreducible representation, here of the PG, and preserves the TR symmetry of the normal state by construction.

By contrast, the intra-band $(d + id)\alpha_0$ pairing, where α_0 is the identity matrix in the band basis, is a linear superposition of two irreducible representations.

In general, the α_0 matrix in band space would correspond to an identity τ_0 matrix in orbital space. The $d + id$ pairing spontaneously breaks both PG and TR symmetries. Therefore, it is a natural analog of ^{3}He -A, which is typically described in terms of equal-spin $p_x + ip_y$ pairing. This phase spontaneously breaks both rotational and TR-symmetries of the normal state as illustrated by Eq. 5 of Supplementary Note 2. The band and spin matrices in the ^{3}He -A and $d + id$ cases are analogous.

In the first subsection, we discussed how $d + d$ differs from ^{3}He -B due mainly to the discrete versus continuous symmetries of the two, respectively. This kind of difference also exists between $d + id$ and ^{3}He -A. The latter spontaneously breaks both angular momentum and spin *continuous* rotational symmetries down to a $U_{L_z-\phi} \times U_{S_z}$ group of independent rotations in each sector about preferred axes (Supplementary Note 2). When dipole-dipole interactions are negligible, the directions of either axes are arbitrarily chosen. By contrast, $d + id$ involves a superposition of pairings belonging to two irreducible representations of a discrete PG corresponding to fixed symmetry axes. Additionally, in ^{3}He -A, the two components, p_x and p_y are exactly degenerate, and there is only a single transition temperature T_c. By contrast, in $d + id$, the two d-components are generically non-degenerate, and two stages of phase transitions are to be expected when the temperature is varied.

In spite of clear differences, the formal similarities between ^{3}He -B and $d + d$ and likewise between ^{3}He -A and $d + id$, which are due to the presence of non-trivial matrix structure, are intriguing. In this sense, ^{3}He provides both a well-established parallel and a prototype for the emergence and description of the effects of non-trivial matrix structure in unconventional singlet SCs.

Given the venerable status of superfluid ^{3}He -B, we believe that revealing the above connections elevates the status of the $d + d$ spin-singlet pairing state. In turn, this connection motivates the consideration of such $d + d$ spin-singlet pairing beyond the context of Fe-based superconductors. Indeed, this leads us to the second part of our work, which is to propose a microscopic pairing state that is capable of understanding the heavy fermion superconductor $CeCu_2Si_2$.

Matrix singlet pairing with spin-orbit coupling: $CeCu_2Si_2$

Another class of multiband superconductors arises in heavy fermion systems, in which quasi-localized *f* electrons hybridize with dispersive *spd*-conduction (*c*) electrons. These include $CeCu_2Si_2$, which is the first-ever discovered unconventional SC[41] and one of the best-studied heavy-fermion SCs. For most of its history, this compound was believed to have a conventional *d*-wave order parameter. Such a conclusion has been supported by inelastic neutron scattering experiments which revealed a spin-resonance peak in the SC state[28] together with angle-resolved resistivity measurements of the upper critical field H_{c2}[66], among others. Remarkably, recent measurements of the specific heat[35] and London penetration depth[34,36] down to lower temperatures indicated a fully-gapped SC state. The apparent contradiction between these different experimental probes is reminiscent of the situation in the Fe-chalcogenide SCs. In those cases, we argued that the fully-gapped but sign-changing $s\tau_3$ provide a natural resolution. An analogous proposal for $CeCu_2Si_2$ is clearly of great interest. Note that a $d + d$ inter- and intra-band pairing directly inspired from the Fe-based cases provides a good fit to the the superfluid-density and specific-heat results in $CeCu_2Si_2$[24,34].

Objective and outline of the subsection. Here, we construct the analog of the $s\tau_3$ pairing for $CeCu_2Si_2$. For reasons that will become clear, we shall refer to this state as $s\Gamma_3$ to indicate the associated non-trivial pairing matrix, as in the case of the Fe-based SCs.

We consider the pairing between the composite heavy quasiparticles in terms of simultaneous *f-f*, *f-c*, and *c-c* pairing in the original electron basis prior to hybridization. Of the three, *f-f* pairing is expected to be the strongest, reflecting the more localized nature of the heavy bands. The albeit weaker *f-c* and *c-c* pairing terms will be important, especially when they are involved in creating a pairing component that opens a gap.

In contrast to the case of the Fe-based SC, an important ingredient for constructing pairing states in a heavy fermion metal such as $CeCu_2Si_2$ is that SOC plays a 0th-order role. The local orbital and spin DOFs transform simultaneously under PG operations. This imposes additional constraints on any matrix associated with the local DOF. Due to the large SOC, the local *f*-electron manifold splits as a consequence of the crystal field. The resulting multiplets, which are labeled according to the irreducible representations of D_{4h}, play a role analogous to that of the $d_{xz/yz}$ orbitals in the Fe-based SC case.

A number of experiments[67,68] as well as LDA+DMFT studies[69] have indicated that one of the Γ_7 doublets of the crystal-field split $^2F_{5/2}$ local electron is the dominant contribution to the heavy FS sheets. The lowest-lying excited states of the *f* electron are composed of a Γ_6 and another Γ_7 doublet. Our analysis will also involve Γ_6 Wannier orbitals of the conduction electron states near the Fermi energy, and these Wannier orbitals will hybridize with the excited Γ_6 *f*-level and thereby makes it a small but nonzero component in the ground-state manifold.

In this subsection, we will use these DOFs to advance a matrix pairing state, $s\Gamma_3$, which transforms in B_{1g} under D_{4h}. To clarify the involved DOFs, we also discuss the character table of the D_{4h} point group and its irreducible representations and construct the conduction-electron Γ_6 Wannier orbitals from the Cu 3*d* orbitals.

Spin-orbital coupled local states. Our aim is to propose a minimal symmetry-allowed candidate for $CeCu_2Si_2$ which has properties similar to that of $s\tau_3$ in the Fe-based cases. By construction, such a state must belong to one of the single-component double-valued irreducible representations of D_{4h}, as required by strong SOC. To illustrate, the even-parity double-valued irreducible representation Γ_1^+ is the analog of A_{1g}, while Γ_3^+ is the analog of B_{1g}. The latter is our prime candidate.

Either *f* or *c* electrons originate from an odd-spin state and therefore transform as either Γ_6 or Γ_7 representations of the PG. A minimal structure for combined local orbital-spin DOF is determined by a 2×2 matrix Σ. This matrix must belong to a non-trivial irreducible representation of the PG; *e.g.*, it must change sign under a C_{4z} rotation. To ensure that the rotation properties are determined exclusively by the local orbital-spin DOF, the pairing must be a product between the non-trivial orbital-spin matrix and a form-factor belonging to the identity representation. In addition to the matrix structure of the local DOF, the pairing matrix must also incorporate *c*, *f* indices.

Thus, a minimal order-parameter is a 4×4 matrix. We consider singlet, parity-even pairing exclusively. Hence, candidate pairing matrices must be *odd under exchange and TR-invariant*. For simplicity, we restrict our discussion to pairings which are even under *f-c* exchange. This necessarily implies that Σ is *anti-symmetric*. Furthermore, as the Σ matrix can transform under inversion, we only consider pairings between electrons belonging to irreducible representations of identical parity. Following the notation used previously, possible candidates are chosen to be of the form

$$\hat{\Delta}(\mathbf{k}) = \Delta g(\mathbf{k})\hat{\Sigma} \otimes \hat{\Xi}. \tag{11}$$

The components of the local-DOF multiplet are determined by the 2×2 Σ matrix while the *f*, *c* nature of the paired electrons is given by the 2×2 Ξ matrix. As in the more familiar case of full spin rotational symmetry, the matrix elements of the Σ matrices are effective Clebsch–Gordan coefficients adapted to the cases of discrete PG symmetry[70].

Conventional B_{1g} *pairing*. We first consider candidates on the Γ_7^- ground-state doublet. The superscript denotes odd parity under inversion. Although these naturally correspond to *f-f* pairing involving the Γ_7 ground-state local multiplet, they also cover possible *f-c* pairings with *c* electrons which belong to the same representation. In the latter case, the *c* electrons would correspond to *p*-type linear-superposition of Wannier orbitals. The tensor product of two such doublets decomposes into the irreducible representations of D_{4h} as[70]

$$\Gamma_7^- \times \Gamma_7^- = \Gamma_1^+ + \Gamma_2^+ + \Gamma_5^+. \tag{12}$$

Here, $\Gamma_{1,2}^+$ are one-dimensional representations which are analogous to the A_{1g} and B_{2g} in the absence of SOC[70]. The two-dimensional Γ_5^+ is analogous to the xz, yz (E_g) doublet. Following Ref. [70], the matrices corresponding to each of the three $\Gamma_{1,2,5}^+$ representations are:

$$\Sigma_{\Gamma_1} = \frac{\mathrm{i}}{\sqrt{2}}\sigma_2 \tag{13}$$

$$\Sigma_{\Gamma_2} = -\frac{\mathrm{i}}{\sqrt{2}}\sigma_1 \tag{14}$$

$$\Sigma^{(5)}_{\Gamma_5,x} = \frac{\mathrm{i}}{\sqrt{2}}\sigma_3 \tag{15}$$

$$\Sigma^{(5)}_{\Gamma_5,y} = \frac{1}{\sqrt{2}}\sigma_0. \tag{16}$$

The σ's are standard Pauli matrices. Recall that for *f-f* or symmetric *f-c* pairings, we require Σ to be anti-symmetric. The only choice is Σ_{Γ_1} which transforms as the trivial representation. This matrix is the analog of simple singlet-pairing in the standard BCS case and is invariant under all PG operations. It is clear that *f-f* or symmetric *f-c* singlet pairing on the Γ_7^- manifold does not support any non-trivial structure in the local DOF. This contrasts with the Fe-based case, where the absence of SOC allowed for all τ matrices in the xz, yz manifold.

We can construct a standard *d*-wave pairing belonging to the Γ_3 representation which is analogous to a B_{1g} representation without SOC. We do so by choosing $g(\mathbf{k}) = d_{x^2-y^2}(\mathbf{k})$ and $\hat{\Sigma} = \Sigma_{\Gamma_1}$ in Eq. (11). Likewise, $\hat{\Xi}$ can be chosen to be proportional to either Ξ_1 or $(1/2)(\Xi_0 - \Xi_3)$, where Ξ_0 and $\Xi_{1,3}$ denote identity and Pauli matrices, respectively. The two cases correspond to *f-c* and *f-f* pairing, respectively.

Matrix B_{1g} *pairing*. We next consider pairing between electrons belonging to distinct Γ_7^- and Γ_6^- manifolds. This can correspond to *f-f* pairing between electrons belonging to the Γ_7^- ground-state and *f* electrons belonging to the excited Γ_6^- manifolds, respectively. Alternately, it can denote *f-c* pairing between Γ_7^- *f*-electrons and Γ_6^- conduction *c* electrons. Further below, we illustrate how intra-unit cell linear combinations of Cu 3*d* states in the presence of SOC can form bases for Γ_6^- conduction electrons. The product states decompose as[70]

$$\Gamma_6^- \times \Gamma_7^- = \Gamma_3^+ + \Gamma_4^+ + \Gamma_5^+. \tag{17}$$

The corresponding matrices are[70]

$$\Sigma_{\Gamma_3} = \frac{\mathrm{i}}{\sqrt{2}}\chi_2 \tag{18}$$

$$\Sigma_{\Gamma_2} = -\frac{\mathrm{i}}{\sqrt{2}}\chi_1 \tag{19}$$

$$\Sigma_{\Gamma_5,x} = \frac{1}{\sqrt{2}}\chi_0 \tag{20}$$

$$\Sigma_{\Gamma_5,y} = \frac{\mathrm{i}}{\sqrt{2}}\chi_3. \tag{21}$$

The χ's are Pauli matrices. Note however that they represent different DOF and thus transform differently under the PG. Therefore, one should not confuse the meaning of the χ Pauli matrices defined in this case with those of the $\Gamma_7 - \Gamma_7$ case discussed previously. The only anti-symmetric matrix is Σ_{Γ_3}. It transforms as the Γ_3^+ irrep of D_{4h} and is an analog of the τ_3 matrix in the Fe-based cases. Moreover, this matrix is invariant under TR. We conclude that a counterpart of the $s\tau_3$ pairing for $CeCu_2Si_2$ is an *s-wave pairing belonging to the sign-changing* Γ_3 *representation, or* $s\Gamma_3$ *pairing*:

$$\hat{\Delta}(\mathbf{k}) = \Delta s(\mathbf{k}) i\chi_2 \otimes \hat{\Xi}, \tag{22}$$

where $s(\mathbf{k})$ corresponds to a *s*-wave form factor which transforms according to the Γ_1^+ trivial irrep. $s\Gamma_3$ pairing, which involves electrons belonging to different irreducible representations due to the Γ_3 matrix, is necessarily non-local, and thus vanishes when $\mathbf{r}_{\mathrm{Relative}} = 0$, where $\mathbf{r}_{\mathrm{Relative}}$ is the distance between two paired electrons. Therefore, we do not restrict the *s*-wave form factor to be of sign-changing form. The form of the Ξ matrix differs depending on either *f-f* or *f-c* pairings. In the *f-c* case it can be chosen to be proportional to a Ξ_1 Pauli matrix. In the $f - f$ case, it can be made proportional to a $\Xi_0 - \Xi_3$ matrix. In either case, the gap is determined by the amplitude and form factor only similarly to what happens for $s\tau_3$. In a multiband model of $CeCu_2Si_2$[34], this pairing produces a full gap.

On general grounds, the non-trivial Γ_7-Γ_6 pairing in either *f-f* or *f-c* cases is likely weaker than the Γ_7-Γ_7 *f-f* pairing. However, there are cases where such Γ_7-Γ_6 contributions can be important. Consider a dominant Γ_7-Γ_7 *f-f* pairing corresponding to a *d*-wave state with nodes along the FS. An admixture of non-trivial pairing either from *f-c* or from *f-f* involving the excited local manifold can open a gap. While we can also consider non-trivial pairing terms in the *c-c* sector, these are expected to be weaker than their *f-f* and *f-c* counterparts. Likewise, other candidates with non-trivial orbital-spin structure can be obtained if we relax some of our assumptions such as the symmetry of the *f-c* terms under exchange. We reserve a detailed analysis of these cases for future work.

Our candidate Γ_7-Γ_6, $s\Gamma_3$ pairing represents an $s\tau_3$ analog for $CeCu_2Si_2$. As in the Fe-based cases, the structure of the local DOF allows a natural interpolation between simple $s-$ and $d-$ wave states. Such a pairing can in principle reconcile the difficulties in interpreting the more recent experimental results.

We note that the Γ_6^- conduction electrons which enter the matrix B_{1g} pairing likely originate from Cu 3*d* orbitals (see below). Indeed, several experiments[24,71,72] have indicated that the strongest suppression of T_c occurs upon substituting Cu by non-magnetic impurities. Our matrix B_{1g} pairing candidate, which involves Γ_6^- conduction electrons from 3*d* Cu states, is naturally consistent with these findings.

Similar to the Fe-chalcogenide case, for unitary pairing we expect the $s\Gamma_3$ pairing in the band basis to contain the intraband a_3 and interband a_1 components. Each must be in *d*-wave state, with the form factor of the intraband a_3 being $d_{x^2-y^2}$. Thus, the $s\Gamma_3$ pairing realizes a $d + d$ multiband pairing. Importantly, the $d + d$ pairing does not break either PG or TR symmetries of the Hamiltonian.

As discussed in the first subsection, we expect that the $s\Gamma_3$ matrix-pairing will coexist with a conventional *d*-wave pairing below T_c since they both belong to the same Γ_3 irreducible representation of D_{4h}. The admixture between these will ensure that the SC state preserves both PG and TR-symmetries but also exhibits a gap which is finite everywhere along the FS.

We stress that our analysis is distinguished from the well-known symmetry-based procedure typically considered in the context of heavy-fermion SCs[73]. The latter does not explicitly treat possible non-trivial matrix structures associated with the local DOF. Instead,

Table 1. Character table for the double-valued representations of the tetragonal D_{4h} point group.

D_{4h}	E	$\bar{E}$	$2C_4$	$2\bar{C}_4$	$C_2/\bar{C}_2$	$2C_2'/2\bar{C}_2'$	$2C_2''/2\bar{C}_2''$	I	$\bar{I}$	$2S_4$	$2\bar{S}_4$	$\sigma_h/\bar{\sigma}_h$	$2\sigma_v$	$2\sigma_d/2\bar{\sigma}_d$
Γ_1^+	1	1	1	1	1	1	1	1	1	1	1	1	1	1
Γ_2^+	1	1	1	1	1	−1	−1	1	1	1	1	1	−1	−1
Γ_3^+	1	1	−1	−1	1	1	−1	1	1	−1	−1	1	1	−1
Γ_4^+	1	1	−1	−1	1	−1	1	1	1	−1	−1	1	−1	1
Γ_5^+	2	2	0	0	−2	0	0	2	2	0	0	−2	0	0
Γ_6^+	2	−2	$\sqrt{2}$	$-\sqrt{2}$	0	0	0	2	−2	$\sqrt{2}$	$-\sqrt{2}$	0	0	0
Γ_7^+	2	−2	$-\sqrt{2}$	$\sqrt{2}$	0	0	0	2	−2	$-\sqrt{2}$	$\sqrt{2}$	0	0	0
Γ_1^-	1	1	1	1	1	1	1	−1	−1	−1	−1	−1	−1	−1
Γ_2^-	1	1	1	1	1	−1	−1	−1	−1	−1	−1	−1	1	1
Γ_3^-	1	1	−1	−1	1	1	−1	−1	−1	1	1	−1	−1	1
Γ_4^-	1	1	−1	−1	1	−1	1	−1	−1	1	1	−1	1	−1
Γ_5^-	2	2	0	0	−2	0	0	−2	−2	0	0	2	0	0
Γ_6^-	2	−2	$\sqrt{2}$	$-\sqrt{2}$	0	0	0	−2	2	$-\sqrt{2}$	$\sqrt{2}$	0	0	0
Γ_7^-	2	−2	$-\sqrt{2}$	$\sqrt{2}$	0	0	0	−2	2	$\sqrt{2}$	$-\sqrt{2}$	0	0	0

the order-parameters are generically classified according to the irreducible representations of the various PGs in the context of a LG analysis. In our case, we have focused on the non-trivial role of the local DOF.

Irreducible representations of D_{4h}. To expound on the local DOFs, we now turn to the character table for the double-valued representations of the tetragonal D_{4h} point group, showing it in Table 1.

We follow the conventions of Ref. [70]. E represents the identity, C_n are rotations about z by $2\pi/n$, while C_2' and C_2'' are π rotations about x, y and $(-x, y), (x, y)$ axes, respectively. I denotes inversion. S_4 indicates a C_4 rotation about z followed by a reflection in the xy plane perpendicular to this axis. σ_h, σ_v, and σ_d are reflections through the xy, xz and yz, and diagonal-z planes, respectively.

In the presence of SOC, the double-valued, even-parity irreducible representations Γ_{1-5}^+ correspond to the single-valued $A_{1g}, A_{2g}, B_{1g}, B_{2g}$, and E_g representations, respectively in the absence of SOC. Likewise, the odd-parity Γ_{1-5}^- correspond to the $A_{1u}, A_{2u}, B_{1u}, B_{2u}$, and E_u representations. Γ_6^+ and Γ_7^+ transform as spinors and product of spinors and linear combinations of Γ_{1-4}^+ and similarly for the odd-parity Γ_6^- and Γ_7^-.

Typical bases for representations relevant to this work are $\Gamma_3^+ : x^2 - y^2$, $\Gamma_4^+ : xy$, $\Gamma_5^+ : xz, yz$. For odd-parity representations we mention $\Gamma_1^- : (x^2 - y^2)xyz$, $\Gamma_3^- : xyz$, $\Gamma_6^- : \Gamma_6^+ \times \Gamma_1^-$ and $\Gamma_7^- : \Gamma_7^+ \times \Gamma_3^-$.

Γ_6^- *conduction electrons*. Previously, we discussed matrix B_{1g} pairing between Γ_6^- c -electrons and Γ_7^- f-electrons. In this subsection, we illustrate how linear combinations of intra-unit-cell Cu 3d orbitals in the presence of SOC provide Γ_6^- conduction electron states. We consider crystal field-split $d_{x^2-y^2}$ Cu orbitals for simplicity although similar constructions are possible for other orbitals.

Consider one of the two Cu planes in the unit cell of $CeCu_2Si_2$[69]. The Cu sites are located halfway along the edges of a plaquette as illustrated in Fig. 5.

The linear combinations of the four orbitals at the Cu sites

$$p_x = d^{(4)}_{x^2-y^2} - d^{(2)}_{x^2-y^2} \tag{23}$$

$$p_y = d^{(1)}_{x^2-y^2} - d^{(3)}_{x^2-y^2} \tag{24}$$

transform as an (x, y) doublet under the D_{4h} point group. Consequently, (p_x, p_y) belong to a two-component Γ_5^- irreducible

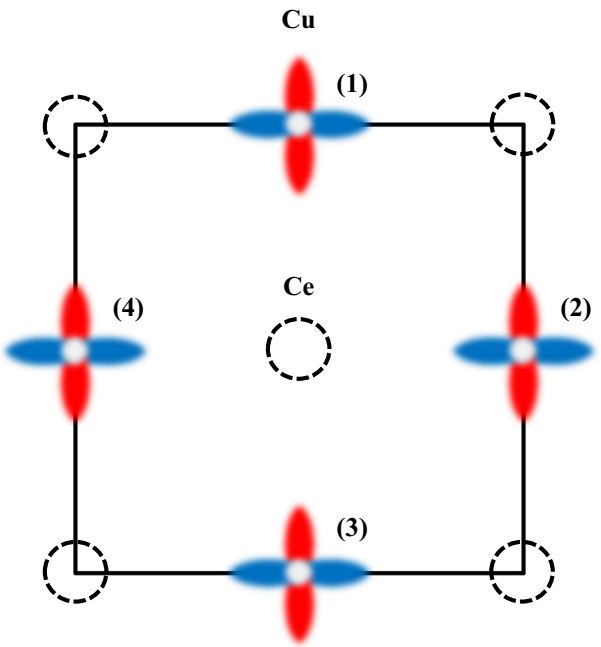

Fig. 5 Single Cu plane in the unit cell of $CeCu_2Si_2$. The four sites labeled (1) − (4) correspond to Cu $d_{x^2-y^2}$ orbitals in the plane. The dashed-line circles represent the Ce sites projected onto the Cu-plane.

representation. We further include the local spin-1/2 DOF which belongs to a Γ_6^+ irreducible representation[70]. From the direct-product states of p-orbital linear combinations and spinor states $\phi_{\pm 1/2}$ we can construct states which belong to Γ_6^- representation[70]:

$$\Psi_{\Gamma_6^-;1/2} = \frac{\mathrm{i}}{\sqrt{2}}[p_x + \mathrm{i}\, p_y]\phi_{-1/2} \tag{25}$$

$$\Psi_{\Gamma_6^-;-1/2} = \frac{\mathrm{i}}{\sqrt{2}}[p_x - \mathrm{i}\, p_y]\phi_{1/2}, \tag{26}$$

where SOC was taken into account. Similar states can be constructed in the remaining Cu plane. The symmetric linear combination between Γ_6^- states in both Cu planes likewise belongs to Γ_6^- doublet.

DISCUSSION

Recent experiments in multiband Fe-based and heavy-fermion SCs are inconsistent with either simple *s*- or *d*-wave pictures, with no conclusive evidence for time reversal symmetry breaking. We argued for alternatives which can interpolate between the two simple cases without breaking the PG and TR symmetries via pairings with non-trivial matrix-structure in the orbital DOF. We discussed how matrix singlet pairings can emerge in unconventional SCs.

To support our general arguments, we considered the specific context of the Fe-based SCs. We present microscopic results showing that the phase difference of the intra-band $d_{x^2-y^2}$ and inter-band d_{xy} pairing components to be either 0 or π. This $d+d$ pairing is the band basis equivalent of the $s\tau_3$ form in the orbital basis, and is an irreducible B_{1g} representation of the (tetragonal D_{4h}) PG. We demonstrate that this $d+d$ singlet pairing state is well defined, by showing that it can be compared and contrasted with the more familiar $d+id$ state in a way analogous to how the well-defined B-phase in the case of superfluid ^{3}He is measured against the equally well-known A-phase. The $d+d$ pairing state allows for the reconcillation between seemingly contradictory experimental observations.

Non-trivial orbital structure can be relevant to unconventional SCs beyond the Fe-based family. To illustrate this, we constructed a pairing analogous to $s\tau_3$ for the heavy-fermion $CeCu_2Si_2$ using general group-theoretical arguments. This $s\Gamma_3$ pairing state is also expected to have a $d+d$ pairing structure in the band basis. It provides a natural theoretical basis to understand the striking low-temperature properties recently measured in the superconducting state of $CeCu_2Si_2$.

In these $d+d$ pairing states, the anti-commuting nature of the two pairing components leads to their contributing to the single-particle excitation spectrum through an addition in quadrature, making it a fully-gapped superconducting state. The formation of the gap is connected to the energetic stabilization of such a state over a range of microscopic parameters. These results lead us to suggest that $d-$wave superconductors of strongly correlated multiorbital systems will inherently have a fully-gapped Fermi surface, even though the gap can be very small.

Note added

During the reviewing process of this manuscript, Ref. [74] appeared with the results of recent x-ray spectroscopy experiments in $CeCu_2Si_2$ that support the $s\Gamma_3$ matrix pairing proposed here for $CeCu_2Si_2$. The $s\Gamma_3$ pairing includes paired Γ_7 *f*-electrons and Γ_6 conduction electrons. As the latter must hybridize with the excited Γ_6 *f*-electron states, a small but nonzero mixture of Γ_6 *f*-electrons is expected in the ground-state manifold. This mixture was shown for $CeCu_2Si_2$ in Ref. [74].

METHODS

Pairing channels of the five-orbital $t-J_1-J_2$ model

We present our results for the five-orbital $t-J_1-J_2$ model of the alkaline Fe-selenides[17]. The leading pairing amplitudes at zero-temperature are shown in Fig. 3 as functions of $J_1^{xz/yz}/J_2^{xz/yz}$. Exchange interactions in the *xz*/*yz* sector are identical for the two orbitals. $J_2^{xz/yz}=1/2$ in units of the bandwidth while the exchange interactions for d_{xy} orbital are 5 times smaller. Interactions in the remaining orbitals are ignored. J_1 and J_2 refer to their values for the *xz*/*yz* sector. For small and large values of the tuning parameter, $s_{x^2y^2}\tau_0, A_{1g}$ and $d_{x^2-y^2}\tau_0, B_{1g}$ orbital-trivial pairings are dominant. In the interval $0.8\le J_1/J_2\le 1$, the $s_{x^2y^2}\tau_3$ pairing with non-trivial orbital structure is dominant with sub-leading $d_{x^2-y^2}\tau_0$ channel. The abrupt change around $J_1/J_2\approx 0.75$ is due to a transition from dominant A_{1g} to B_{1g} channels which become quasi-degenerate in this region. For the FS considered here, large J_2 favors dominant $s_{x2y2}\tau_0$, A_{1g} while large J_1 favors $d_{x2-2y2}\tau_0$, B_{1g} channels, respectively.

The form factors for the pairing terms have the standard expressions

$$s_{x^2+y^2}(\mathbf{k})=\frac{1}{2}\left[\cos(k_x a)+\cos(k_y a)\right] \tag{27}$$

$$s_{x^2y^2}(\mathbf{k})=\cos(k_x a)\cos(k_y a) \tag{28}$$

$$d_{x^2-y^2}(\mathbf{k})=\frac{1}{2}\left[\cos(k_x a)-\cos(k_y a)\right] \tag{29}$$

$$d_{xy}(\mathbf{k})=\sin(k_x a)\sin(k_y a). \tag{30}$$

Five-orbital $t-J_1-J_2$ model and solution method

The pairing instabilities in the different symmetry channels of the alkaline Fe-selenides were obtained via a five-orbital $t-J_1-J_2$ model:

$$H=-\sum_{i<j}(t_{ij}^{\alpha\beta}c_{\alpha}^{\dagger}c_{\beta}+\text{h.c.})+\sum_{i,\alpha}(\epsilon_{i\alpha}-\mu)n_i+\sum_{\langle ij\rangle,\alpha,\beta}J_1^{\alpha\beta}\left(\mathbf{S}_{i\alpha}\cdot\mathbf{S}_{j\beta}-\tfrac{1}{4}n_{i\alpha}n_{j\beta}\right)+\sum_{\langle\langle ij\rangle\rangle,\alpha,\beta}J_2^{\alpha\beta}\left(\mathbf{S}_{i\alpha}\cdot\mathbf{S}_{j\beta}-\tfrac{1}{4}n_{i\alpha}n_{j\beta}\right), \tag{31}$$

where i,j indices cover all of the sites of a two-dimensional square lattice and $\alpha,\beta\in\{1,\ldots 5\}$ represent the $d_{xz}, d_{yz}, d_{x^2-y^2}, d_{xy}$, and d_{z^2} orbitals, respectively. The parameters of the model are specified in Ref. [64]. Different orbitals exhibit varying degrees of correlations, such that the exchange couplings are orbital dependent. More specifically, intra-orbital exchange couplings for the $d_{x^2-y^2}$ and d_{z^2} orbitals are set to zero. Both NN and next-NN (NNN) exchange couplings are equal in the $d_{xz/yz}$ sector and are larger by a factor of 5 than the exchange couplings in the d_{xy} sector. Inter-orbital exchanges have a small effect[17] and are neglected here.

The interactions are decoupled in the particle-particle channel and the model is solved at $T=0$ within a self-consistent approach. The double-occupancy constraint is introduced via an effective band renormalization[17,64].

We calculate the intra-orbital, NN and NNN pairing bonds, driven by J_1 and J_2 exchange couplings respectively, along $\hat{\mathbf{x}}$, $\hat{\mathbf{y}}$ and $\hat{\mathbf{x}}+\hat{\mathbf{y}}$ and $\hat{\mathbf{x}}-\hat{\mathbf{y}}$ respectively as

$$\Delta_{\mathbf{e},\alpha\alpha}=\frac{1}{2}\left\langle c^{\dagger}_{\mathbf{R}_i\alpha\uparrow}c^{\dagger}_{\mathbf{R}_i+\mathbf{e}\alpha\downarrow}-c^{\dagger}_{\mathbf{R}_i\alpha\downarrow}c^{\dagger}_{\mathbf{R}_i+\mathbf{e}\alpha\uparrow}\right\rangle \tag{32}$$

where $\mathbf{e}\in\{\hat{\mathbf{x}},\hat{\mathbf{y}},\hat{\mathbf{x}}+\hat{\mathbf{y}},\hat{\mathbf{x}}-\hat{\mathbf{y}}\}$, $\mathbf{R}_i$ is a site vector, and α is an orbital index. The NN and NNN pairing bonds enter the pairing part of a Nambu Hamiltonian via

$$\Delta_{\mathbf{k},\alpha\alpha}=\sum_{\mathbf{e}}J_{\mathbf{e}}\cos(\mathbf{k}\cdot\mathbf{e}) \tag{33}$$

The *dimensionless pairing amplitudes* reported in the Results section are obtained by taking appropriate linear combinations of the NN and NNN pairing bonds. As such, the procedure does not bias towards any particular pairing channel. In addition, there are no approximations for the shape of the FS, and the pairing bonds are determined via averages where the momentum summation is over the entire Brillouin zone. The calculation is initiated with a random set of NN and NNN pairing bonds for all of the orbitals and subsequently allowed to converge. The procedure is repeated until a set of 300 converged solutions are obtained. From this set of converged solutions, we select the one which corresponds to the absolute minimum in the associated free-energy. This solution, again obtained without any superfluous conditions, corresponds to the physical solution reported in the manuscript.

Single-orbital $t-J_1-J_2$ model

The Hamiltonian of the single d_{xy} orbital $t-J_1-J_2$ model defined on a 2D square lattice is

$$H=H_{\text{TB}}+J_1\sum_{\langle ij\rangle}\mathbf{S}_i\cdot\mathbf{S}_j+J_2\sum_{\langle\langle ij\rangle\rangle}\mathbf{S}_i\cdot\mathbf{S}_j, \tag{34}$$

where i,j label the lattice sites. The spin-density operators are defined as $\mathbf{S}_i=(1/2)\sum_{ab}c_a^{\dagger}(\mathbf{R}_i)\boldsymbol{\sigma}_{ab}c_b(\mathbf{R}_j)$, where a,b are spin indices.

The TB part is determined by

$$H_{TB}=-t_1\sum_{\langle ij\rangle}\sum_a c_a^{\dagger}(\mathbf{R}_i)c_a(\mathbf{R}_j)-t_3\sum_{\langle\langle ij\rangle\rangle}\sum_a c_a^{\dagger}(\mathbf{R}_i)c_a(\mathbf{R}_j)-\mu\sum_i\sum_a c_a^{\dagger}(\mathbf{R}_i)c_a(\mathbf{R}_i). \tag{35}$$

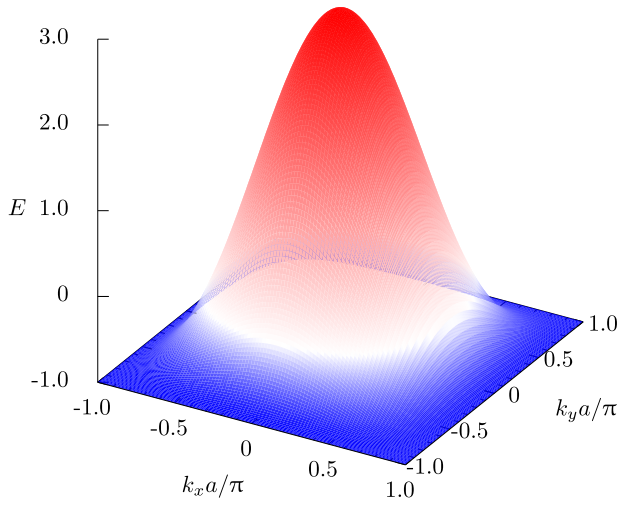

Fig. 6 Dispersion corresponding to Eq. (36) in units of $2|t_1|$ with $t_1 = 2t_3 = -0.5$. $\mu \approx -0.3$ ensures the FS shown in Fig. 7 near half-filling.

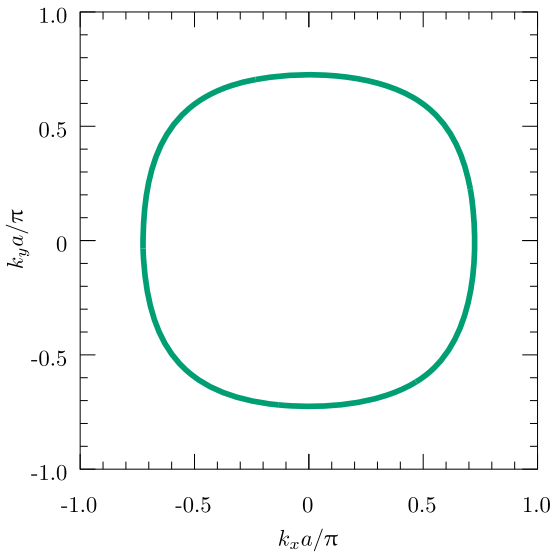

Fig. 7 Hole-like FS for a single-orbital d_{xy} model. Here, the system is close to half-filling.

The band is determined by

$$\epsilon(\mathbf{k}) = -2t_1\left[\cos(k_x a) + \cos(k_y a)\right] - 4t_3 \cos(k_x a)\cos(k_y a) - \mu, \quad (36)$$

where a is the NN distance.

The TB coefficients are chosen as $t_1 = 2t_3 = -0.5$. The resulting band is shown in Fig. 6. Near half-filling we take $\mu \approx -0.3$ to obtain the FS shown in Fig. 7.

We implicitly take into account the renormalization of the bandwidth near half-filling by considering a large, fixed effective $J_2 = -2t_1 = 1$ while J_1 is allowed to vary. We decouple the exchange interactions in the pairing channels. The model is solved using the methods of Refs. [17,64] near half-filling.

DATA AVAILABILITY

The data that support the findings of this study are available from the corresponding author upon reasonable request.

CODE AVAILABILITY

The codes that support the findings of this study are available from the corresponding author upon reasonable request.

Received: 28 June 2020; Accepted: 2 December 2020;
Published online: 05 January 2021

REFERENCES

1. Lee, P. A., Nagaosa, N. & Wen, X.-G. Doping a Mott insulator: physics of high-temperature superconductivity. *Rev. Mod. Phys.* **78**, 17–85 (2006).
2. Scalapino, D. J. A common thread: the pairing interaction for unconventional superconductors. *Rev. Mod. Phys.* **84**, 1383–1417 (2012).
3. Agterberg, D. F., Brydon, P. M. R. & Timm, C. Bogoliubov Fermi surfaces in superconductors with broken time-reversal symmetry. *Phys. Rev. Lett.* **118**, 127001 (2017).
4. Ramires, A., Agterberg, D. F. & Sigrist, M. Tailoring T_c by symmetry principles: the concept of superconducting fitness. *Phys. Rev. B* **98**, 024501 (2018).
5. Kamihara, Y., Watanabe, T., Hirano, M. & Hosono, H. Iron-based layered superconductor La[$O_{1-x}F_x$]FeAs ($x = 0.05 - 0.12$) with $T_c = 26$ K. *J. Am. Chem. Soc.* **130**, 3296–3297 (2008).
6. Johnston, D. C. The puzzle of high temperature superconductivity in layered iron pnictides and chalcogenides. *Adv. Phys.* **59**, 803–1061 (2010).
7. Dai, P. Antiferromagnetic order and spin dynamics in iron-based superconductors. *Rev. Mod. Phys.* **87**, 855–896 (2015).
8. Yi, M., Zhang, Y., Shen, Z.-X. & Lu, D. Role of the orbital degree of freedom in iron-based superconductors. *npj Quantum Materials* **2**, 57 (2017).
9. Si, Q., Yu, R. & Abrahams, E. High-temperature superconductivity in iron pnictides and chalcogenides. *Nat. Rev. Mater.* **1**, 16017 (2016).
10. Wang, F. & Lee, D.-H. The electron-pairing mechanism of iron-based superconductors. *Science* **332**, 200–204 (2011).
11. Hirschfeld, P. J. Using gap symmetry and structure to reveal the pairing mechanism in Fe-based superconductors. *C. R. Physique* **17**, 197–231 (2016).
12. Yi, M. et al. Observation of temperature-induced crossover to an orbital-selective Mott phase in $A_xFe_{2-y}Se_2$ (A=K, Rb) superconductors. *Phys. Rev. Lett.* **110**, 067003 (2013).
13. Yu, R. & Si, Q. Orbital-selective Mott phase in multiorbital models for alkaline iron selenides $\mathbf{K}_{1-x}Fe_{2-y}Se_2$. *Phys. Rev. Lett.* **110**, 146402 (2013).
14. Yu, R., Zhu, J.-X. & Si, Q. Orbital-selective superconductivity, gap anisotropy, and spin resonance excitations in a multiorbital t-J_1-J_2 model for iron pnictides. *Phys. Rev. B* **89**, 024509 (2014).
15. Yin, Z. P., Haule, K. & Kotliar, G. Spin dynamics and orbital-antiphase pairing symmetry in iron-based superconductors. *Nat. Phys.* **10**, 845–850 (2014).
16. Ong, T., Coleman, P. & Schmalian, J. Concealed d-wave pairs in the $s \pm$ condensate of iron-based superconductors. *Proc. Natl Acad. Sci. USA* **113**, 5486–5491 (2016).
17. Nica, E. M., Yu, R. & Si, Q. Orbital-selective pairing and superconductivity in iron selenides. *npj Quant. Mater.* **2**, 24 (2017).
18. Kreisel, A. et al. Orbital selective pairing and gap structures of iron-based superconductors. *Phys. Rev. B* **95**, 174504 (2017).
19. Hu, H., Yu, R., Nica, E. M., Zhu, J.-X. & Si, Q. Orbital-selective superconductivity in the nematic phase of FeSe. *Phys. Rev. B* **98**, 220503 (2018).
20. Hu, L.-H., Johnson, P. D. & Wu, C. Pairing symmetry and topological surface state in iron-chalcogenide superconductors. *Phys. Rev. Res.* **2**, 022021 (2020).
21. Zhang, C. et al. Measurement of a double neutron-spin resonance and an anisotropic energy gap for underdoped superconducting $NaFe_{0.985}Co_{0.015}As$ using inelastic neutron scattering. *Phys. Rev. Lett.* **111**, 207002 (2013).
22. Sprau, P. O. et al. Discovery of orbital-selective Cooper pairing in FeSe. *Science* **357**, 75–80 (2017).
23. Shibauchi, T., Hanaguri, T. & Matsuda, Y. Exotic superconducting states in FeSe-based materials. *J. Phys. Soc. Jpn.* **89**, 102002 (2020).
24. Smidman, M. et al. Interplay between unconventional superconductivity and heavy-fermion quantum criticality: $CeCu_2Si_2$ versus $YbRh_2Si_2$. *Philos. Mag.* **98**, 2930–2963 (2018).
25. Park, J. T. et al. Magnetic resonant mode in the low-energy spin-excitation spectrum of superconducting $Rb_2Fe_4Se_5$ single crystals. *Phys. Rev. Lett.* **107**, 177005 (2011).
26. Friemel, G. et al. Reciprocal-space structure and dispersion of the magnetic resonant mode in the superconducting phase of $Rb_xFe_{2-y}Se_2$ single crystals. *Phys. Rev. B* **85**, 140511 (2012).
27. Eschrig, M. The effect of collective spin-1 excitations on electronic spectra in high-T_c superconductors. *Adv. Phys.* **55**, 47–183 (2006).
28. Stockert, O. et al. Magnetically driven superconductivity in $CeCu_2Si_2$. *Nat. Phys.* **7**, 119–124 (2011).
29. Maier, T. A., Graser, S., Hirschfeld, P. J. & Scalapino, D. J. d-wave pairing from spin fluctuations in the $K_xFe_{2-y}Se_2$ superconductors. *Phys. Rev. B* **83**, 100515 (2011).

30. Mou, D. et al. Distinct Fermi surface topology and nodeless superconducting gap in a $(Tl_{0.58}Rb_{0.42})Fe_{1.72}Se_2$ superconductor. *Phys. Rev. Lett.* **106**, 107001 (2011).
31. Wang, X.-P. et al. Strong nodeless pairing on separate electron Fermi surface sheets in (Tl, K)$Fe_{1.78}Se_2$ probed by ARPES. *Europhy. Lett.* **93**, 57001 (2011).
32. Xu, M. et al. Evidence for an *s*-wave superconducting gap in $K_xFe_{2-y}Se_2$ from angle-resolved photoemission. *Phys. Rev. B* **85**, 220504 (2012).
33. Wang, X.-P. et al. Observation of an isotropic superconducting gap at the Brillouin zone centre of $Tl_{0.63}K_{0.37}Fe_{1.78}Se_2$. *Europhys. Lett.* **99**, 67001 (2012).
34. Pang, G. et al. Fully gapped d-wave superconductivity in $CeCu_2Si_2$. *Proc. Natl Acad. Sci. USA* **115**, 5343–5347 (2018).
35. Kittaka, S. et al. Multiband superconductivity with unexpected deficiency of nodal quasiparticles in $CeCu_2Si_2$. *Phys. Rev. Lett.* **112**, 067002 (2014).
36. Yamashita, T. et al. Fully gapped superconductivity with no sign change in the prototypical heavy-fermion $CeCu_2Si_2$. *Sci. Adv.* **3**, e1601667 (2017).
37. Grinenko, V. et al. Superconductivity with broken time-reversal symmetry inside a superconducting s-wave state. *Nat. Phys.* **16**, 789–794 (2020).
38. Zaki, N., Tsvelik, A.M., Wu, C. & Johnson, P. Time reversal symmetry breaking in the Fe-chalcogenide superconductors. Preprint at https://arxiv.org/abs/1907.11602 (2019).
39. Goswami, P., Nikolic, P. & Si, Q. Superconductivity in multi-orbital $t-J_1-J_2$ model and its implications for iron pnictides. *Europhys. Lett.* **91**, 37006 (2010).
40. Wang, X. et al. Constraints imposed by symmetry on pairing operators for the iron pnictides. *Phys. Rev. B* **81**, 144509 (2010).
41. Steglich, F. et al. Superconductivity in the presence of strong Pauli paramagnetism: $CeCu_2Si_2$. *Phys. Rev. Lett.* **43**, 1892 (1979).
42. Mathur, N. D. et al. Magnetically mediated superconductivity in heavy fermion compounds. *Nature* **394**, 39–43 (1998).
43. Gegenwart, P., Si, Q. & Steglich, F. Quantum criticality in heavy-fermion metals. *Nat. Phys.* **4**, 186–197 (2008).
44. Thompson, J. D. & Fisk, Z. Progress in heavy-fermion superconductivity: Ce115 and related materials. *J. Phys. Soc. Jpn* **81**, 011002 (2012).
45. Ran, S. et al. Nearly ferromagnetic spin-triplet superconductivity. *Science* **365**, 684–687 (2019).
46. Pustogow, A. et al. Constraints on the superconducting order parameter in Sr_2RuO_4 from oxygen-17 nuclear magnetic resonance. *Nature* **574**, 72–75 (2019).
47. Ishida, K. et al. Spin-triplet superconductivity in Sr_2RuO_4 identified by ^{17}O Knight shift. *Nature* **396**, 658–660 (2008).
48. Mackenzie, A. P. & Maeno, Y. The superconductivity of Sr_2RuO_4 and the physics of spin-triplet pairing. *Rev. Mod. Phys.* **75**, 657–712 (2003).
49. Rice, T. M. & Sigrist, M. Sr_2RuO_4: an electronic analogue of ^3He? *J. Phys. Condens. Matter* **7**, L643–L648 (1995).
50. Kallin, C. & Berlinsky, A. J. Is Sr_2RuO_4 a chiral p-wave superconductor? *J. Phys. Condens. Matter* **21**, 164210 (2009).
51. Ramires, A. & Sigrist, M. Superconducting order parameter of Sr_2RuO_4: a microscopic perspective. *Phys. Rev. B* **100**, 104501 (2019).
52. Huang, W., Zhou, Y. & Yao, H. Exotic Cooper pairing in multiorbital models of Sr_2RuO_4. *Phys. Rev. B* **100**, 134506 (2019).
53. Raghu, S., Qi, X.-L., Liu, C.-X., Scalapino, D. J. & Zhang, S.-C. Minimal two-band model of the superconducting iron oxypnictides. *Phys. Rev. B* **77**, 220503 (2008).
54. Si, Q. & Abrahams, E. Strong correlations and magnetic frustration in the high T_c iron pnictides. *Phys. Rev. Lett.* **101**, 076401 (2008).
55. Daghofer, M., Nicholson, A., Moreo, A. & Dagotto, E. Three orbital model for the iron-based superconductors. *Phys. Rev. B* **81**, 014511 (2010).
56. Zhou, Y., Chen, W.-Q. & Zhang, F.-C. Symmetry of superconducting states with two orbitals on a tetragonal lattice: application to $LaFeAsO_{1-x}F_x$. *Phys. Rev. B* **78**, 064514 (2008).
57. Nicholson, A. et al. Pairing symmetries of a hole-doped extended two-orbital model for the pnictides. *Phys. Rev. B* **85**, 024532 (2012).
58. Lv, W., Moreo, A. & Dagotto, E. B_{1g}-like pairing states in two-leg ladder iron superconductors. *Phys. Rev. B* **88**, 094508 (2013).
59. Graser, S., Maier, T. A., Hirschfeld, P. J. & Scalapino, D. J. Near-degeneracy of several pairing channels in multiorbital models for the Fe pnictides. *New J. Phys.* **11**, 025016 (2009).
60. Chubukov, A. V., Vafek, O. & Fernandes, R. M. Displacement and annihilation of Dirac gap nodes in *d*-wave iron-based superconductors. *Phys. Rev. B* **94**, 174518 (2016).
61. Agterberg, D. F., Shishidou, T., O'Halloran, J., Brydon, P. M. R. & Weinert, M. Resilient nodeless *d*-wave superconductivity in monolayer FeSe. *Phys. Rev. Lett.* **119**, 267001 (2017).
62. Leggett, A. J. A theoretical description of the new phases of liquid ^3He. *Rev. Mod. Phys.* **47**, 331–414 (1975).
63. Vollhardt, D. & Wölfle, P. The superfluid phases of Helium 3 (Taylor & Francis, London, 1990).
64. Yu, R., Goswami, P., Si, Q., Nikolic, P. & Zhu, J.-X. Superconductivity at the border of electron localization and itinerancy. *Nat. Commun.* **4**, 2783 (2013).
65. Sachdev, S. Quantum phase transitions of correlated electrons in two dimensions. *Phys. A* **313**, 252–283 (2002).
66. Vieyra, H. A. et al. Determination of gap symmetry from angle-dependent H_{c2} measurements on $CeCu_2Si_2$. *Phys. Rev. Lett.* **106**, 207001 (2011).
67. Goremychkin, E. A. & Osborn, R. Crystal-field excitations in $CeCu_2Si_2$. *Phys. Rev. B* **47**, 14280 (1993).
68. Rueff, J.-P. et al. Absence of orbital rotation in superconducting $CeCu_2Ge_2$. *Phys. Rev. B* **91**, 201108 (2015).
69. Pourovskii, L. V., Hansmann, P., Ferrero, M. & Georges, A. Theoretical prediction and spectroscopic fingerprints of an orbital transition in $CeCu_2Si_2$. *Phys. Rev. Lett.* **112**, 106407 (2014).
70. Koster, G. F. Properties of the thirty-two point groups (Cambridge, Mass., M.I.T. Press, 1963).
71. Spille, H., Rauchschwalbe, U. & Steglich, F. Superconductivity in $CeCu_2Si_2$: dependence of T_c on alloying and stoichiometry. *Helv. Phys. Acta* **56**, 165–177 (1983).
72. Yuan, H. Q. et al. Observation of two distinct superconducting phases in $CeCu_2Si_2$. *Science* **302**, 2104–2107 (2003).
73. Sigrist, M. & Ueda, K. Phenomenological theory of unconventional superconductivity. *Rev. Mod. Phys.* **63**, 239–311 (1991).
74. Amorese, A. et al. Possible multi-orbital ground state in $CeCu_2Si_2$. Preprint at https://arxiv.org/abs/2010.01836 (2020).

ACKNOWLEDGEMENTS

We thank Pengcheng Dai, J. C. Séamus Davis, Onur Erten, Haoyu Hu, Andrea Severing, Michael Smidman, Frank Steglich, L. Hao Tjeng, Roxanne Tutchton, Ming Yi, Rong Yu, Huiqiu Yuan, Jian-Xin Zhu, and Gertrud Zwicknagl for useful discussions. This work has been supported by ASU startup grant (E.M.N.) and by the DOE BES Award No. DE-SC0018197 and the Robert A. Welch Foundation Grant No. C-1411 (Q.S.). We acknowledge the hospitality of Center for Nonlinear Studies at Los Alamos National Laboratory, where part of this work was initiated. Q.S. acknowledges the support by a Ulam Scholarship of the Center for Nonlinear Studies and the hospitality of the Aspen Center for Physics (NSF Grant no. PHY-1607611).

AUTHOR CONTRIBUTIONS

Both authors contributed equally in the design of this study, in the acquisition and interpretation of the supporting data, and in the drafting of the text.

COMPETING INTERESTS

The authors declare no competing interests.

ADDITIONAL INFORMATION

Supplementary information is available for this paper at https://doi.org/10.1038/s41535-020-00304-3.

Correspondence and requests for materials should be addressed to E.M.N. or Q.S.

Reprints and permission information is available at http://www.nature.com/reprints

Publisher's note Springer Nature remains neutral with regard to jurisdictional claims in published maps and institutional affiliations.